

# Synchronisation in an AC-Driven Artificial Quantum Neuron\*

F228019<sup>†</sup>

(Dated: January 16, 2026)

Based on the artificial quantum neuron model proposed by Potter et al [1], exhibiting self-sustained voltage oscillations via an Andronov–Hopf bifurcation under DC bias. This paper extends the model to examine forced dynamics by adding a sinusoidal term to the input voltage. Numerical simulations are shown to exhibit classical non-linear effects, including phase-locking, Arnold tongue structures, and quasiperiodicity, as a function of drive frequency and amplitude. Synchronisation is characterised in the form of limit cycles in Bloch vector space and power spectral densities with frequency locking to the drive. At high drive powers, the onset of aperiodic dynamics is seen, revealing the possibility of complex behaviour beyond quasiperiodicity. These findings aim to contribute towards comprehending forced responses in quantum memristive neurons and shine light on controlling quantum neuromorphic circuits externally.

## I. INTRODUCTION

The memristor was first theoretically proposed in 1971 by Leon Chua [2] as the fourth fundamental passive circuit element, alongside resistors, capacitors and inductors, because its behaviour could not be replicated using only the other three in a circuit, linking flux and charge. Chua was later proved correct in 2008 by HP Labs who produced the first real memristive device using positive oxygen vacancies in titanium dioxide crystals [3], finding that memristive behaviour becomes much more prominent at nanoscales. After 37 years, the connection between Chua's theory and HP Labs' realised device revived interest in memristors.

Memristors exhibit a special characteristic by which the conductance of the device is determined by the history of the current through it. This behaviour produces a non-linear voltage response, shown in a pinch-hysteresis loop for input current and voltage across the device [4], demonstrating a difference in Voltage despite the same current passing through it. Unlike a capacitor or inductor, a memristor stores information in the form of its internal state, rather than energy. Memristors can also be classified based on the retention of its internal state – either volatile, non-volatile or both [5]. This paper will be investigating a device that exhibits behaviour of a diffusive (volatile) memristor [6], meaning that the conductive pathways will dissipate over time if no external voltage is applied [7]. This adaptive behaviour is particularly needed to replicate biological synapse [8]; specifically, the ability to “forget” its internal state if it is not stimulated.

Inherent memory and processing capabilities in a single element have found it being widely adopted in neuromorphic (brain-like) computer architecture [9]. With the onset of AI and the incredible demand for computational power [10-11] bringing increased interest to alternatives like neuromorphic architecture- a hardware implemen-

tation of an artificial neural network [12]. Transporting information between memory and processing units in von-Neumann architecture poses the largest limit to this architecture by increasing energy consumption and speed [13]. By merging memory and logic into the same physical component, memristive technologies are enabling in-memory computing and huge parallel data processing. An example of this can already be seen from implementing a memristor-based resistive RAM (RRAM) on a logic circuit to act as an on-chip storage [14]. Or memristor crossbars, reducing the number of devices needed for large matrix multiplications, a core technique in AI, by performing analogue computations rather than fetching weights from DRAM [15].

One of the benefits is the small size of memristors, however this also means it is a small step moving to nano scales where quantum effects become more prevalent [16]. Despite memristive technology still not being commercially used, there have been several investigations into quantum memristors for future scalability of the device, popular methods being quantum-optic [17-18] and carbon quantum dot [19-20] due to their unique electrical properties potentially fixing issues that memristors currently experience [21]. Quantum features such as superposition, entanglement and decoherence control enrich system behaviour in quantum neuromorphic architectures.

Classical memristive circuits already tend to produce complex non-linear behaviours like multi-stability, bifurcations and chaos [22-23]. Features that can be harnessed but need to be controlled for a reliable neuromorphic system [21]. A previous study into coupling two artificial neurons via memristors proves synchronisation of spiking behaviour depending on the memristor's conductance [24]. This shows that it is possible to influence these behaviours, to ensure control over their implementation.

Recently, Potter et al [1] introduced a classical artificial neuron circuit that utilises a quantum memristive device. A two-level charged quantum particle acts as a shuttle for electrons to tunnelling through from one terminal to the other. As the electron jumps onto the shuttle the quantum state of the particle changes and dynamically alters the conductance of the device, pro-

---

\* A footnote to the article title

† Also at Physics Department, Loughborough University.

ducing a characteristic I-V loop. Furthermore, the device produces self-sustained voltage oscillations as environmental decoherence and pumping voltage counteract, making an Andronov-Hopf bifurcation [25]. These exotic behaviours closely mimic core aspects of a biological neuron [26], making it a great system to study for future applications in neuromorphic computing.

The investigation on the system previously have focussed solely on a static DC input, however neurons in neuromorphic computers receive spikes and parameters of these spike, such as time, shape and magnitude, could represent encoded data [15]. Moreover, it is important to understand oscillating input signals for this memristive device as it produces its own voltage oscillations, so by linking multiple together, oscillating current would be received. Non-linear systems, when driven periodically, have already been shown to produce synchronisation, beating and possibly even chaos [22].

This study rebuilds the system described by Potter et al and extends it to investigate forced dynamics of the quantum memristor in an artificial neuron circuit by adding a sinusoidal signal to the input signal. It aims to reproduce crucial system dynamics demonstrated by Potter et al [1], followed by mapping out synchronisation region for varying voltage amplitudes and angular frequencies to demonstrate phase locking and characterise synchronised and unsynchronised regimes with potential to produce chaotic dynamics.

## II. THEORETICAL BACKGROUND: ARTIFICIAL NEURON SYSTEM DYNAMICS

The artificial neuron circuit proposed theoretically by Potter et al [1] was used in this investigation. The circuit consists of a resistor that is in series to a parallel capacitor and quantum memristor, Fig.1(a). A key feature of memristive systems are the feedback relationship between voltage and conductance. This relationship for the conductance and voltage of the device can be derived using standard Ohm and Kirchoff laws applied to the artificial neural circuit (AppendixA for the derivation).

$$\tau_c \frac{dV_m}{dt} = V_{\text{ext}} - [1 + R_{\text{ext}}G_{\text{dev}}] V_m, \quad (1)$$

$R_{\text{ext}}$  is the external resistance,  $C_{\text{ext}}$  is the capacitance of the circuit,  $\tau_c = R_{\text{ext}}C_{\text{ext}}$  is the circuit's characteristic time scale,  $V_m$  is the voltage across the memristor,  $V_{\text{ext}}$  represents the applied constant DC voltage and  $G_{\text{dev}}$  is the memristor conductance.

The quantum memristor, proposed by Potter et al [1], is modelled as a charged quantum particle that shuttles between two oppositely charged electrodes, Fig. 1. The quantum particle is constrained to the ground state and first excited state to form a qubit by the particle's superposition between both energy levels. Electrons tunnel "on and off" the shuttle from one electrode to the

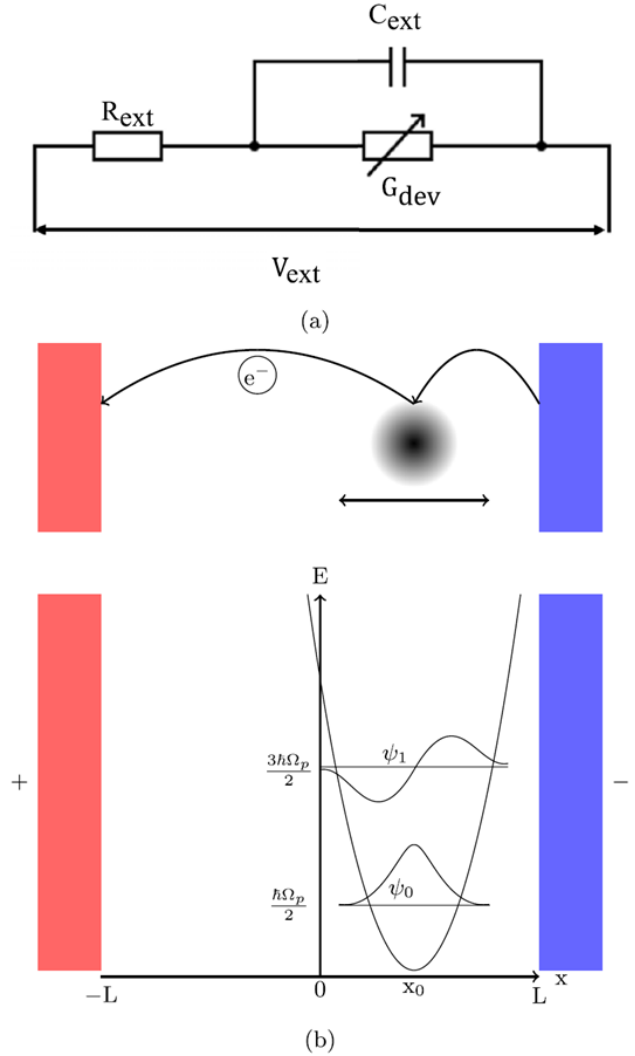


FIG. 1. (a) The artificial neuron circuit diagram with  $G_{\text{dev}}$  representing the conductance of the quantum memristive device. (b) Diagram depicting the the electron's tunnelling process dependant on the quantum particle's position relative to the electrodes and the energy level of the particle modelled as a simple harmonic oscillator at the ground and the first excited state.

other, affecting not only the quantum state of the particle but also the tunnelling conductance because it depends on the particles position,  $x_0$ , and therefore its quantum state. Originally, Savel'ev et al [28] modelled the shuttle particle classically and therefore have approximated the conductance in a classical system.

$$G = \operatorname{sech}\left(\frac{x}{\lambda}\right) \cdot \frac{1}{R_0} \quad (2)$$

The minimal resistance is denoted as  $R_0$ , the position of the particle,  $x$ , and  $\lambda$  being the tunnelling length for the electron. This assigns the particle a definite position but in the quantum regime the particle is in a superposition of states - therefore the position is probabilistic. To Cal-

culate the position probabilistically the trace,  $Tr$ , of the density matrix,  $\rho$ , is taken to define the total probability of the system in all possible states. The conductance in this system will be dependent on the present voltage across the device and the Particle's Bloch vector components ( $X$ ,  $Y$ ,  $Z$ ).

$$G = \left\langle \operatorname{sech} \left( \frac{x}{\lambda} \right) \right\rangle \cdot \frac{1}{R_0} = \operatorname{Tr} \left( \rho \cdot \operatorname{sech} \left( \frac{x(V_m)}{\lambda} \right) \right) \cdot \frac{1}{R_0} \quad (3)$$

The expectation value of  $x(V_m)$  is calculated and cross multiplied by the  $2 \times 2$  density matrix,  $\rho$ . The equation is then simplified by the trace,  $Tr$ , to average across the possible states and creates a function dependent on the matrix indices,  $i$  and  $j$ . (see Appendix A for details):

$$F_{i,j}(x_V) = \frac{1}{l \sqrt{2^{i+j} i! j! \pi}} \int_{-\infty}^{\infty} e^{-\frac{\tilde{x}^2}{l^2}} H_i \left( \frac{\tilde{x}}{l} \right) H_j \left( \frac{\tilde{x}}{l} \right) \times \operatorname{sech} \left( \frac{\tilde{x} + x_V}{\lambda} \right) d\tilde{x} \quad (4)$$

Consisting of the electron tunnelling length ( $l$ ), Hermite polynomials ( $H_n$ ) and  $x_V = x_0 - l \cdot \sqrt{2}V$ . For a  $2 \times 2$  matrix this produces 3 unique functions of  $x_V$  because  $F_{0,1} = F_{1,0}$ . The conductance,  $G_{\text{Dev}}$  is therefore a function of  $V$ .

$$G_{\text{DEV}} = \frac{1}{2R_0} \cdot [(1+Z) \cdot F_{0,0}(x_V) + 2X \cdot F_{0,1}(x_V) + (1-Z) \cdot F_{1,1}(x_V)] \quad (5)$$

With an expression for conductance equation (6) is sub-

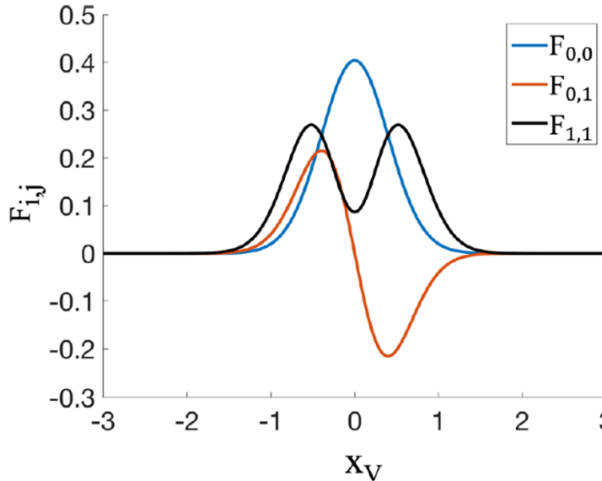


FIG. 2. The plot is  $F_{i,j}(x_V)$  with  $l = 0.5$  and  $\lambda = 0.12$  from Potter et al [1]. The plot shows the different complex behaviours of the function depending on the quantum state and position of the active quantum particle.

stituted into equation (2) to make an ODE for voltage across the memristive device that is now dependent on the voltage  $V$ .

$$\tau_c \frac{dV_m}{dt} = V_{\text{ext}} - \left[ 1 + R_{\text{ext}} \frac{1}{2R_0} \cdot ((1+Z)F_{0,0} + 2XF_{0,1} + (1-Z)F_{1,1}) \right] V_m, \quad (6)$$

In order to understand the behaviour of voltage across the memristor,  $V_m$ , the Bloch vector components ( $X$ ,  $Y$ ,  $Z$ ) are introduced for the two-level density matrix. Potter et al [1] proposed four dimensionless coupled ODEs to describe the full system dynamics.

$$\dot{V} = V_n - \left\{ 1 + \frac{R_n}{2} [(1+Z)F_{0,0}(x_V) + 2XF_{0,1}(x_V) + (1-Z)F_{1,1}(x_V)] \right\} V. \quad (7)$$

This defines a dimensionless instantaneous change in voltage across the memristor,  $\dot{V}$ . The voltage change depends on not only the input voltage,  $V_n$ , but also the current Voltage,  $V$ , a necessity for producing bifurcation dynamics in the Voltage. Increasing or decreasing the input voltage to the same value could produce multiple Voltage values. For consistency parameter values are set, unless explicitly stated, to  $l/L = 0.5$ ,  $x_0/L = 0.8$ ,  $\lambda/L = 0.13$ ,  $\alpha = 1$ , and  $\Omega = 7$ .

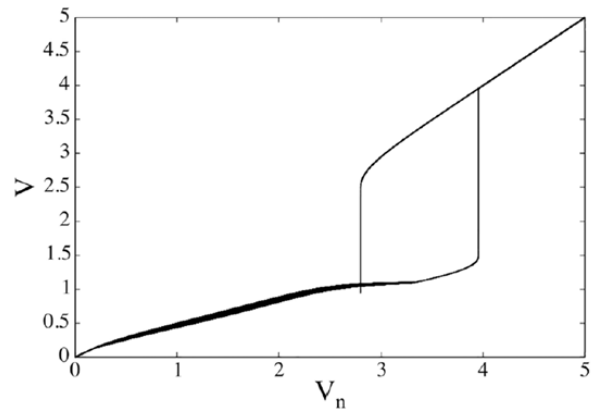


FIG. 3. Potter et al [1] plot the characteristic pinched hysteresis loop found in I-V graphs of memristive systems. As  $V_n$  slowly increases the Voltage follows a slow increase from 0 up to  $V \approx 1$  until  $V_n \approx 4$  where the voltage spikes to  $V \approx 3.5$ , it then slowly increases again. Conversely, decreasing input voltage from 5, a bifurcation occurs at  $V_n \approx 4$  as voltage continues to slowly decrease and instead sharply drop at  $V_n \approx 2.8$ . The graph clearly depicts the dependence of the change in Voltage on its current voltage value.

The Bloch vector components are derived from the initial Hamiltonian. The Hamiltonian is transformed into its two level Hamiltonian matrix and substituted into the Liouville von Neumann equation to describe how the Bloch vector components evolve through time [27] - necessary to understand the voltage ODE.

$$\begin{aligned} \dot{Z} &= -2\dot{V}X - \alpha\Gamma(Z - Z_T), \\ \dot{X} &= \Omega Y + 2\dot{V}Z - \Gamma X, \\ \dot{Y} &= -\Omega X - \Gamma Y, \end{aligned} \quad (8)$$

Potter et al [1] discovered relaxation in  $Z$  must be less than  $2\Gamma$ , where  $X$  and  $Y$  experience the same dephasing rate,  $\Gamma$ . Here  $\alpha$  determines the magnitude of the relaxation, therefore  $\alpha \in [0, 2]$ .  $Z_T$  is a dimensionless thermal equilibrium, derived by Potter et al [1], to determine the dissipation of energy due to heat[29].

Due to dissipation in the Bloch sphere, pumping current into the device can find an equilibrium between losing and gaining energy. The interplay between these two actions produce self-oscillations [30] in the Voltage.

### III. RESULTS AND DISCUSSION

#### A. Reproducing Artificial Neuron Dynamics

The dynamics of the artificial neuron are replicated to ensure simulations accurately characterise the system behaviour before investigation a periodic input signal. Firstly, the conductance, and therefore voltage dynamics,  $V$ , depend on three functions (5) which can be determined by keeping parameters consistent to establish an identical system Fig. 6. The distance to the midpoint between the electrodes in the memristive device is taken as  $L = 1$  for ease of determining parameters. Therefore  $l = 0.5$ ,  $x_0 = 0.8$ ,  $\lambda = 0.13$ ,  $\alpha = 1$ , and  $\Omega = 7$ . By keeping these parameters constant, the three functions,  $F_{0,0}$ ,  $F_{0,1}$ ,  $F_{1,1}$ , are constant in this investigation.

To simulate the Voltage and Bloch vector components evolution through time, fourth order Runge-Kutta is utilised to reduce the truncation error between time steps. The quantum particle self organises on the phase space ( $X$ ,  $Y$ ,  $Z$ ), meaning no matter the initial conditions set for  $X$ ,  $Y$ ,  $Z$ ,  $V$ , given enough time the system will find a either a stable point or cycle. This is displayed in Fig. 7 (a) where despite initially having  $V = 0$  the system tends towards an equilibrium, in this case with a constant voltage. There exist three stable points in the phase space, two fixed at  $X = 0$ ,  $Y = 0$ , and  $Z = 1$  or  $0$ , the top and bottom of the Bloch sphere.

By letting the system stabilise for varying  $V_n$  and by keeping the  $X$ ,  $Y$ ,  $Z$ ,  $V$  components continuous between small increments of  $V_n$ , the system between  $V_n \approx 0.23$  and  $V_n = 3.31$ , seen in Fig. 8. This self-sustained oscillation persists even through the hysteresis loop. By maintaining continuous conditions between  $V_n$  increments Fig. 8 evidences the dependence of  $V$  on its initial conditions before reaching equilibrium for each  $V_n$ .

Due to the behaviour of the Bloch vector components fitting to the surface of Bloch sphere,  $V$  oscillates (as seen in Fig. 7(a)) as it tends to a stable equilibrium, this is not to be mistaken as self-sustained oscillations. This behaviour appears not only in a self-oscillating regime but also for fixed point voltage. A stable  $V$  sinusoidal wave will form (Fig. 9(a)) when a self-oscillation occurs and while the Phase space for fixed  $V$  tends to a stable point, self-oscillations exhibit a stable limit-cycle (seen in Fig. 9(b)), in the phase space. As found by Potter et al

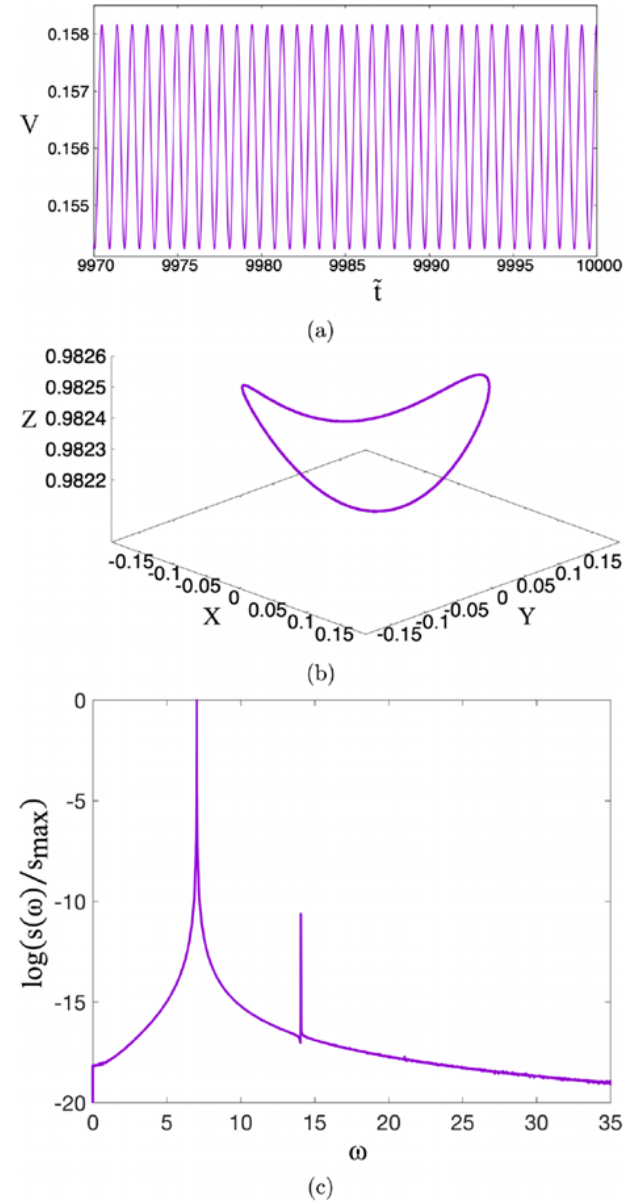


FIG. 4. Potter et al [1] found self oscillations with  $R_n = 5$ ,  $V_n = 0.23$ ,  $\Gamma = 0.1$ ,  $\alpha = 1$ , and  $Z_T = 1$ . (a) The voltage-time plot shows periodic oscillations after  $\tilde{t} = 9970$  despite a static input. (b) The system has reached a stable limit cycle in the Bloch sphere showing that relaxation is involved. This stable loop, displayed in the phase space, is a characteristic of periodic self-oscillations and Andronov Hopf bifurcation. (c) The power spectral density of the self oscillations shows a main angular frequency at  $\omega = 7.0246$ , with smaller second and third harmonics.

[1], the  $V$  oscillation sustain an angular frequency  $\omega = 7.0$  shown as the main frequency at  $V_n = 0.23$ . This is calculated using the Fast Fourier Transform (FFT) in conjunction with periodogram averaging and Hanning windows.

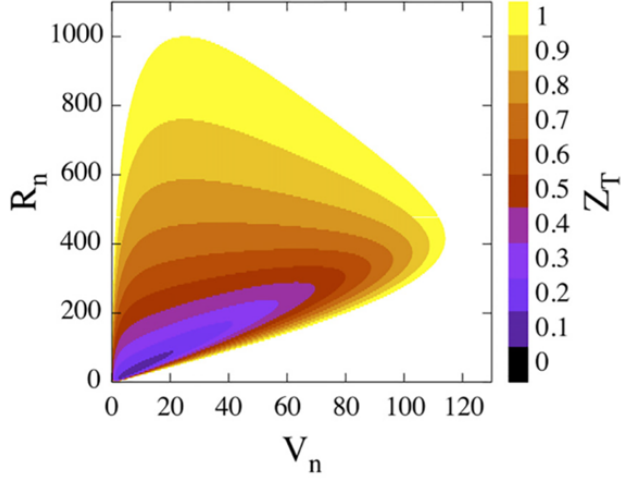
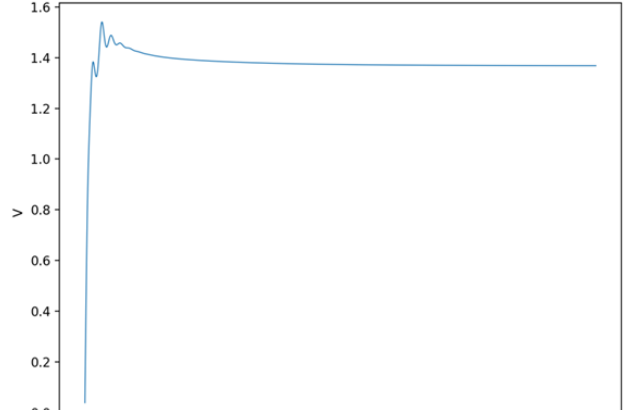
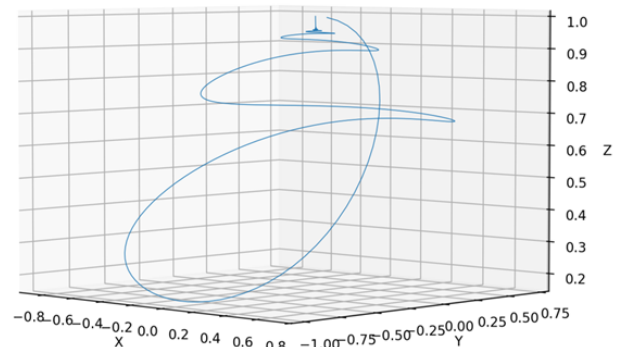


FIG. 5. The plot, by Potter et al [1], depicts regions of oscillation in voltage,  $V$ , with  $\Gamma = 0.1$  and  $\alpha = 1.0$ , across varying dimensionless resistance,  $R_n$ , and applied voltage,  $V_n$ , for different values of thermal equilibrium,  $Z_T$ .  $Z_T$  ranges from 0, representing infinite temperature, to 1 depicting zero temperature. The borders of each region represent the onset of Andronov Hopf bifurcations. It shows a clear correlation between a higher thermal equilibrium, indicated by the colour, and broader range of parameters to experience voltage self-oscillations.



(a)



(b)

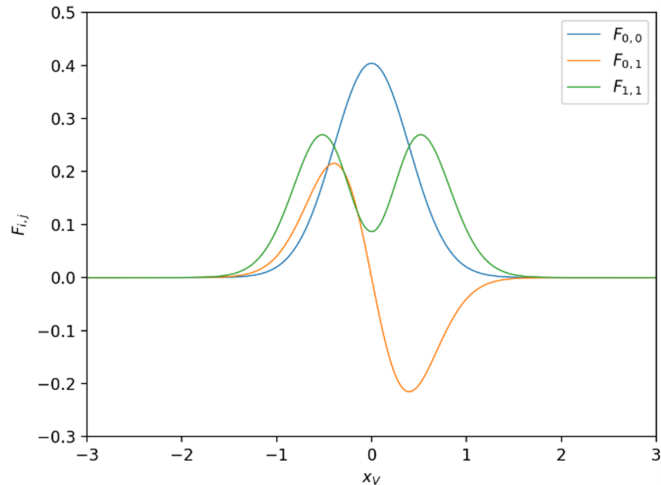


FIG. 6. This plot is a reproduction of Fig. 2. The functions are calculated for  $x_V \in [-3, 3]$  as all three functions have tended to zero by these points, so values past these parameters are assumed to be 0.

FIG. 7. Constant voltage observed when  $R_n = 5$ ,  $V_n = 3.9$  and  $Z_T = 1$  with From initial conditions  $X = 0$ ,  $Y = 0$ ,  $Z = 1$  and  $V = 0$ . (a) Voltage-time graph for  $\tilde{t} \in [0, 50]$ . (b) The evolution of the Bloch vector components through time to reach a fixed point.

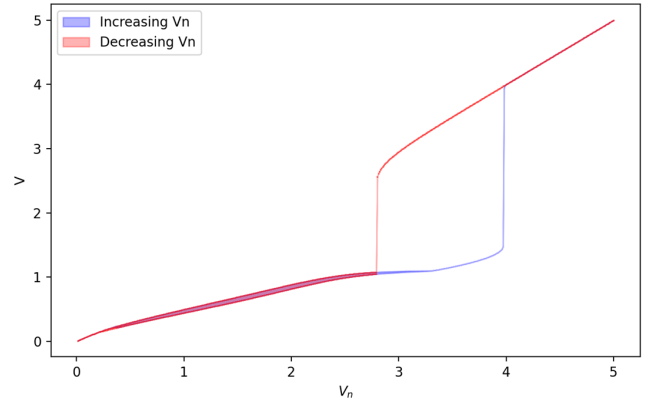


FIG. 8. Stable  $V$  for continuously increasing (blue) and decreasing (red)  $V_n$ . A clear hysteresis loop and Andronov Hopf bifurcation are shown, with the min and max  $V$  plotted so line thickness can indicate  $V$  amplitude.

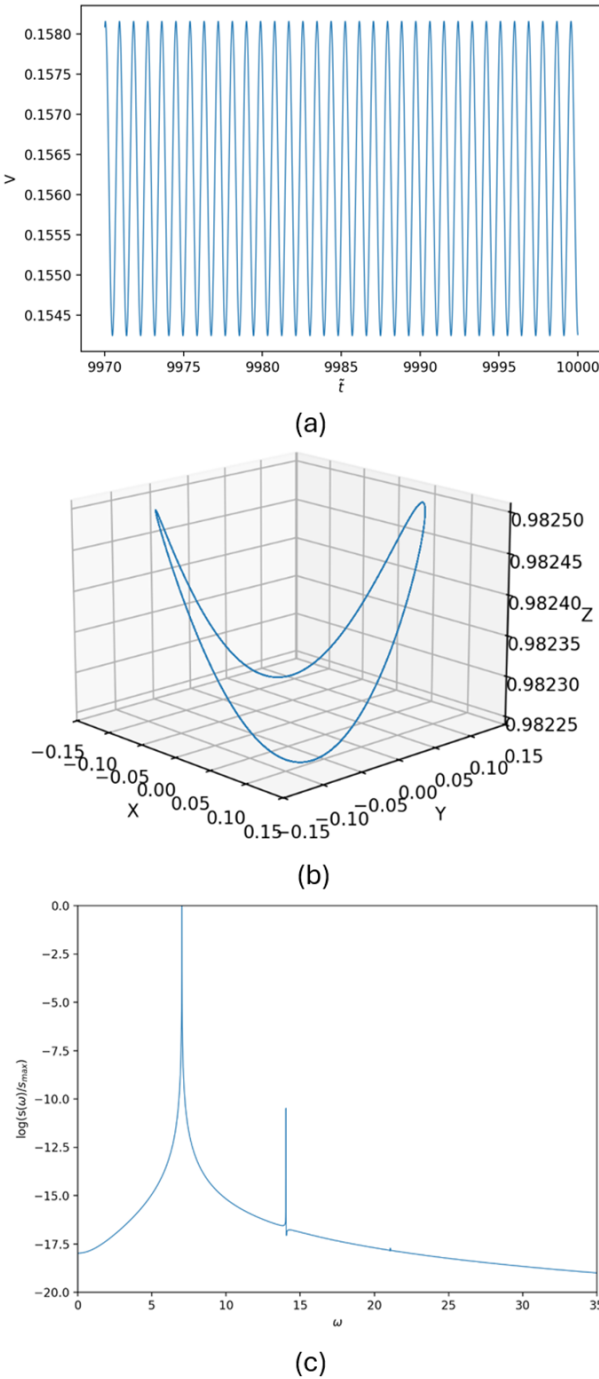


FIG. 9. Self-oscillations observed when  $R_n = 5$ ,  $V_n = 0.23$ ,  $\Gamma = 0.1$ ,  $\alpha = 1$ , and  $Z_T = 1$ . (a) Long term voltage dynamics showing spiking behaviour. (b) Stable limit cycle expected from self-oscillations observed in the phase space. (c) A normalised and averaged power spectrum of oscillations for angular frequency,  $\omega$ .

Finally, regions of  $V_n$  and  $R_n$  were tested for self oscillations and mapped for  $Z_T = 0.3$  and  $Z_T = 0.6$ . The resultant regions match the corresponding regions mapped by Potter et al in Fig. 5. The perimeter of these regions indicate the creation of instability from Andronov

Hopf bifurcations, however this is not displayed precisely due to insufficient simulation time for some variables to achieve equilibrium.

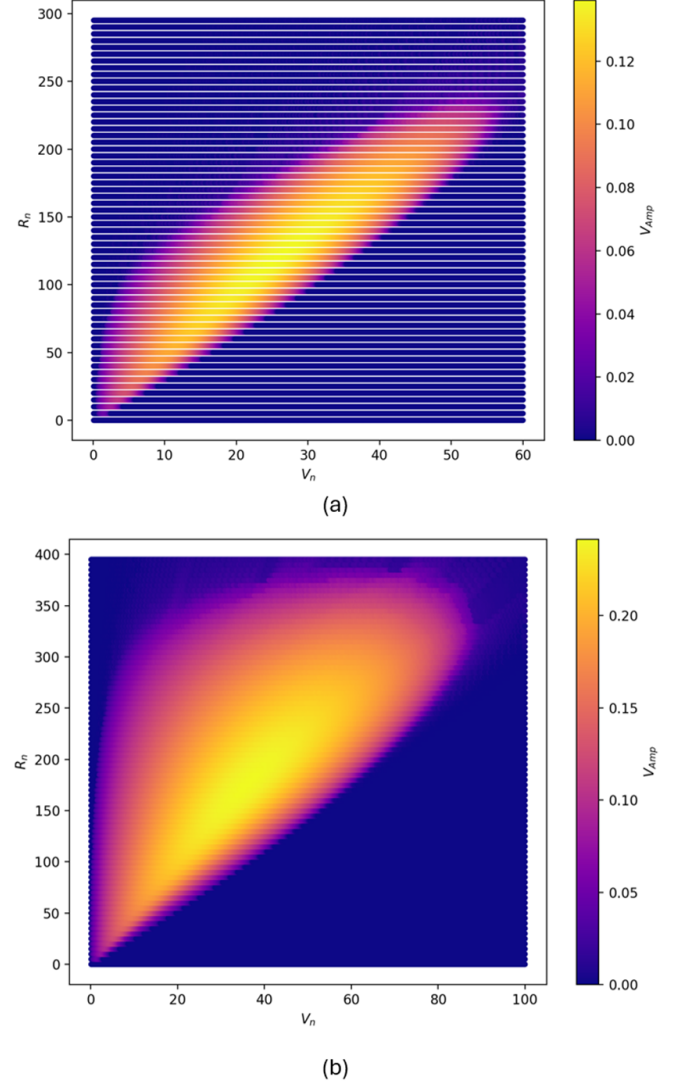


FIG. 10. Regions of voltage,  $V$ , self oscillations achieved for varying  $R_n$  and  $v_n$  and heat map indicating the amplitude of oscillations,  $V_{Amp}$ . (a) Oscillation region for  $Z_T = 0.3$ . (b) Oscillation region for  $Z_T = 0.6$ .

#### IV. SYNCHRONISATION IN AN AC-DRIVEN ARTIFICIAL NEURON

The original system applied a DC signal and produced self-sustained voltage oscillations. This creates a great opportunity to study how the balance between quantum decoherence and energy pumping evolves with a time-dependent input. The system was extended by adding a sinusoidal term to the DC signal.

$$V_n = V_{DC} + V_{Amp} \cdot \sin(\omega \cdot \tilde{t}) \quad (9)$$

This slight addition can provide incite into forcing dynamic such as synchronisation, quasiperiodicity and chaos. The system will use the same parameters established within the DC simulations.

A variety of drive frequencies were simulated with different amplitudes to characterise the transition between self oscillations and a drive-locked behaviour. Synchronisation could be determined by two features. Firstly, the Bloch vector components and voltage converging to a limit cycle and secondly the power spectral density (PSD) only has a single main peak at drive frequency and harmonics of this peak.

The synchronised system shows clear frequency locking of the Voltage to the drive frequency. The voltage-time plots showed a regular, periodic oscillation matching that of the drive frequency(Fig. 11(a)). A stable limit cycle is produced in the phase space (Fig. 11(b)), similarly to that seen from self-oscillations. The PSD graph demonstrates a main frequency,  $\omega = 6.00$  and three subsequent harmonics, completely eliminating any prior frequencies (Fig. 11(c)). These three features strongly implies the drive has forced synchronisation, indicating that voltage frequencies over the device can be controlled.

On the other hand, the unsynchronised system produces classic characteristics of a quasi-periodic oscillation. In the voltage-time plot, the peaks and troughs are clearly oscillating, indicative of beating [30](Fig. (a)). In the phase space a 2-torus shape has formed [37](Fig. 13). The vector trajectory did not close but instead fill the surface of the torus(Fig. 12(b)). The PSD has large peaks at the natural self-oscillation frequency,  $\omega = 7.024$ , and the drive frequency. It also produces a large peak at the difference in the drive and natural frequency at  $\omega \approx 1$ .

The expected shape for synchronisation across  $V_{Amp}$  and drive frequency is a sharp wedge with its point at  $\omega \approx 7$ , known as an Arnold-tongue diagram. In order to investigate the minimum threshold of coupling strength, around the natural self oscillation frequency, for synchronisation to form, the  $V_{Amp}$  was swept until the dominant frequency spike calculated by PSD was the drive frequency. However, as seen in Fig. (c), the dominant frequency switching does not necessitate synchronisation but also appears in in some quasi-periodic regimes.

Fig. was created using this method and does conformed to the hypothesis, with an expected wedge at  $\omega \approx 7$ . What was not expected though was the oscillating shape of onset drive frequency dominance. It remains unknown whether this periodic threshold arises from the synchronisation threshold or the dynamics of the main frequency.

While investigating large  $V_{Amp}$  values I discovered strange behaviour in the phase space, moving away from the expected simple limit-cycle, the trajectories became more erratic (Fig . There is clear breakdown of the stable limit cycle, however they system have not reached chaos as you can see a symmetry in each graph [31].(See appendix E for example chaotic attractors).

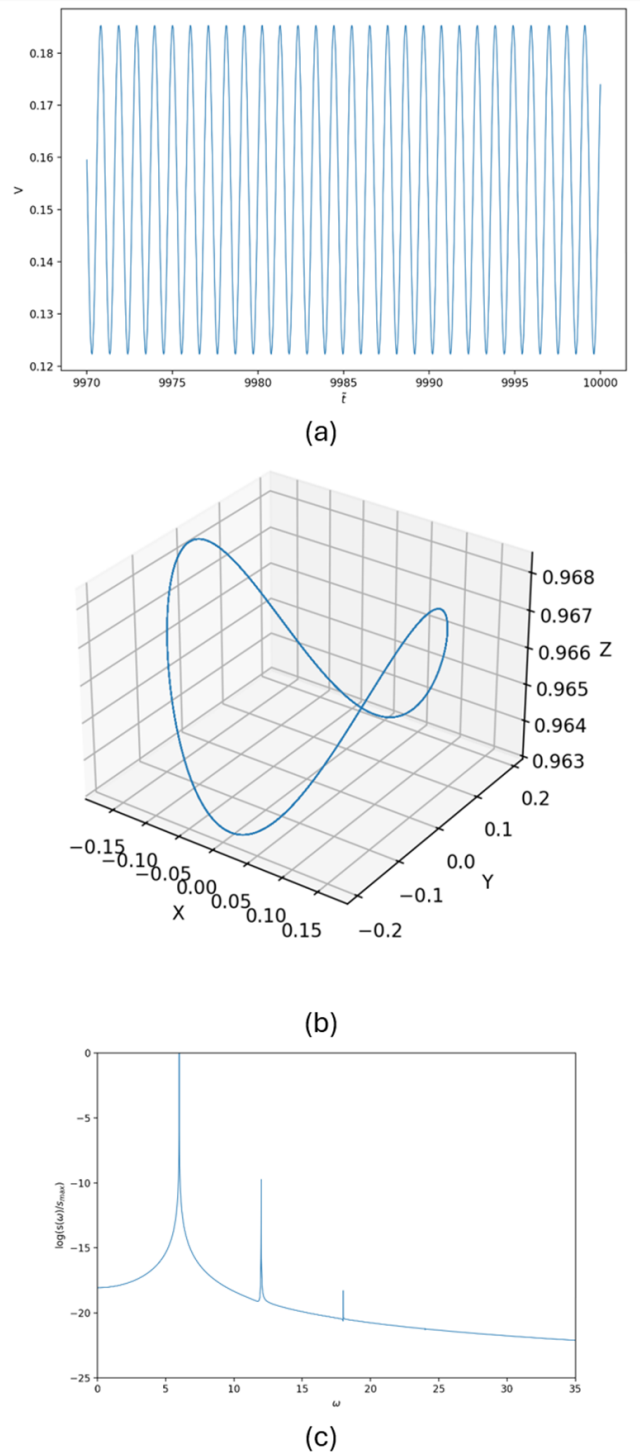
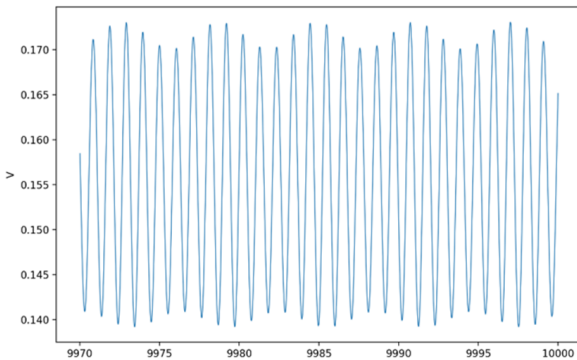
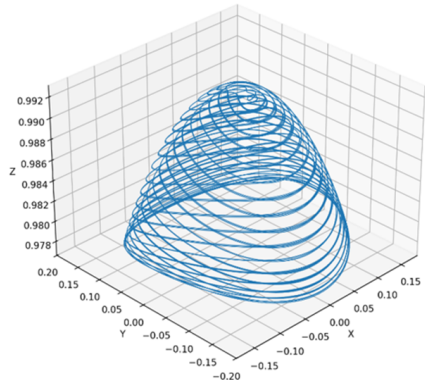


FIG. 11. Synchronisation observed with  $V_{DC} = 0.23$ ,  $\omega = 6.00$  and  $V_{Amp} = 0.2$ . (a) Forcible frequency oscillations in voltage-time. (b) Stable limit cycle in Bloch vector component space. (c) Normalised power spectral density with main frequency at  $\omega = 6.00$ .



(a)



(b)

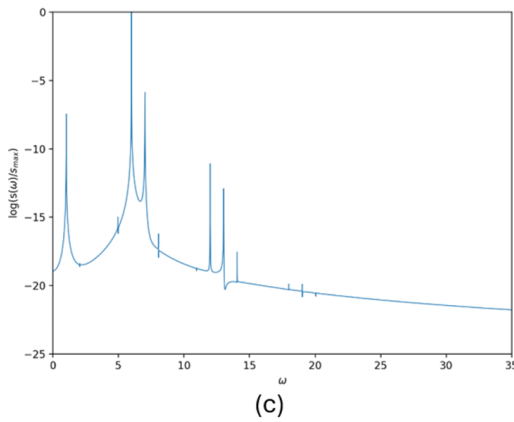


FIG. 12. Quasi-periodicity observed with  $V_{DC} = 0.23$ ,  $\omega = 6.00$  and  $V_{Amp} = 0.1$ . (a) Oscillation beating in voltage-time. (b) A torus has formed in the Bloch vector component space. (c) Normalised power spectral density

## V. CONCLUSION

Applying an oscillating signal within the input voltage could offer a tunable mechanism to control the artificial neuron Oscillating behaviour. The discovery of synchronisation implies that neuron outputs can be externally influenced, an essential tool for incorporation into a large-scale neuromorphic array [32]. This also offers a low-cost

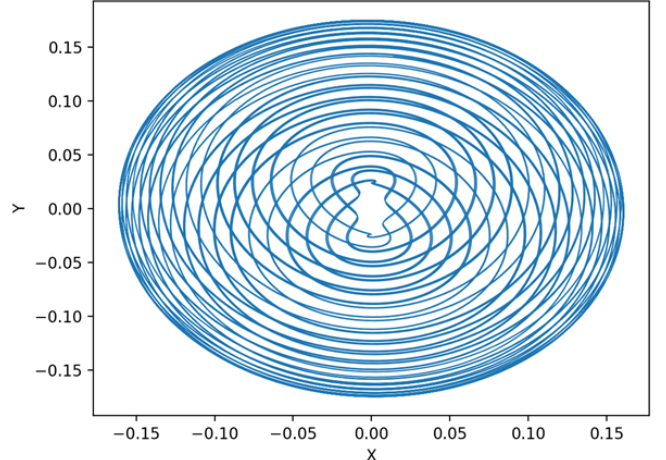
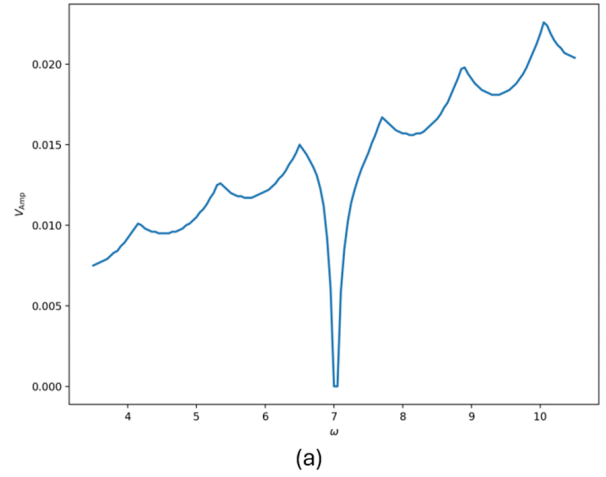
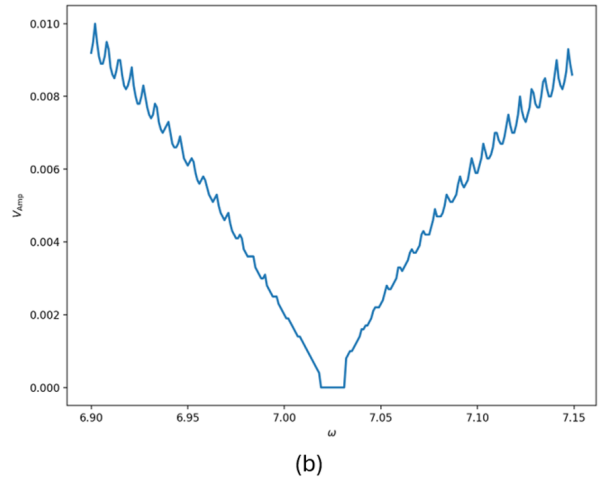


FIG. 13. Quasi-periodicity observed in X-Y Bloch vector space with  $V_{DC} = 0.23$ ,  $\omega = 6.00$  and  $V_{Amp} = 0.1$ .



(a)



(b)

FIG. 14. Quasi-periodicity observed in X-Y Bloch vector space with  $V_{DC} = 0.23$ ,  $\omega = 6.00$  and  $V_{Amp} = 0.1$ .

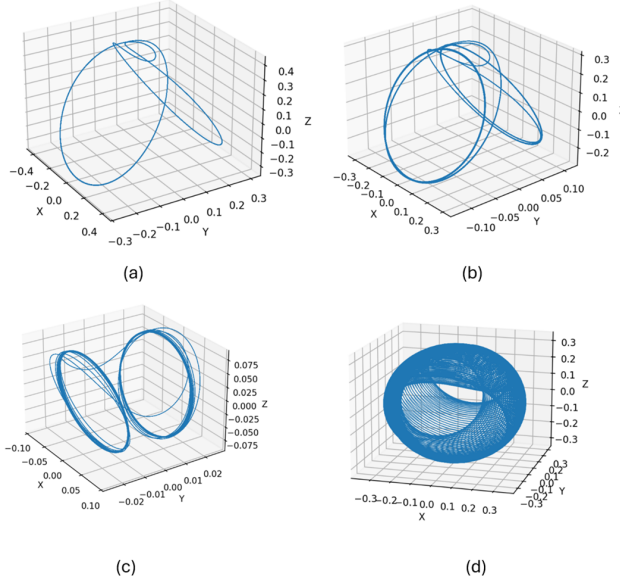


FIG. 15. Extreme input voltage observed in Bloch vector component space. (a)  $V_{DC} = 0.23$ ,  $\omega = 6.00$  and  $V_{Amp} = 10$ . (b)  $V_{DC} = 0.23$ ,  $\omega = 6.00$  and  $V_{Amp} = 20$ . (c)  $V_{DC} = 0.23$ ,  $\omega = 6.00$  and  $V_{Amp} = 100$ . (d)  $V_{DC} = 3.00$ ,  $\omega = 6.00$  and  $V_{Amp} = 10$ .

control mechanism as the system can be switched between autonomous and entrained regimes by merely tuning input parameters.

The qualitative similarity of the behaviour of this quantum neuron and classical entrained oscillators supports the contention that phase-locking, Arnold tongues, and quasiperiodicity are generic characteristics in both systems [30]. The observation that these behaviours are maintained in a quantum-mechanical memristive device with environmental dissipation demonstrates that basic principles of non-linear dynamics stay true even in novel quantum neuromorphic devices.

Although chaos was not the primary focus, the fact that complex, non-periodic dynamics at high detuning and amplitude only serves to reinforce the necessity of understanding and controlling forced dynamics in these systems. In general, the system offers a strong experimental foundation for the investigation of entrainment, resonance, and stability for the development of future neuromorphic hardware based on quantum memristive architecture.

## VI. NOTE

GitHub repository with containing all code used in this investigation

## Appendix A: DERIVATION OF THE VOLTAGE-CONDUCTANCE RELATIONSHIP

Using symbols from the artificial neuron circuit, Fig. 1(a), we can establish an equation between the change on voltage and conductance over the memristive device.

$$\text{Following Ohm's law: } I = \frac{V}{R} = G \cdot V$$

$$\text{Therefore } I_{dev} = G_{dev} \cdot V_{dev}$$

Capacitor and Memristor are in parallel so following Kirchoff's law:  $V_{dev} = V_C$ , where  $V_C$  is the voltage across the capacitor.

$I_{ext} = I_R = I_{dev} + I_C \dots (1)$ , where  $I_R$  is current through the resistor.

$$I_{ext} = I_C = \frac{V_C}{R_{ext}} = \frac{V_{ext} - V_{dev}}{R_{ext}} = I_C + I_{dev} \dots (2)$$

An expression for the current through a capacitor is:

$$I = C \left( \frac{dV}{dt} \right)$$

Therefore we can say,  $I_C = C_{ext} \left( \frac{dV_C}{dt} \right) = C_{ext} \left( \frac{dV_m}{dt} \right) \dots (3)$

Now substitute equations (1) and (3) into equation (2).

$$\frac{V_{ext} - V_{dev}}{R_{ext}} = C_{ext} \frac{dV_{dev}}{dt} + G_{dev} V_{dev}$$

$$R_{ext} C_{ext} \frac{dV_m}{dt} = V_{ext} - V_{dev} - G_{dev} V_{dev} R_{ext}$$

$\tau_C = R_{ext} C_{ext}$ .  $\tau_C$  being the characteristic timescale, or RC constant, that describes the rate a capacitor charges or discharges through a resistor.

Finally,

$$\tau_C \frac{dV_{dev}}{dt} = V_{ext} - (1 + G_{dev} R_{ext}) V_{dev}$$

## Appendix B: LORENZ AND RÖSSLER CHAOTIC ATTRACTORS

The Lorenz attractor (Fig. 16(a)) consists of three coupled ODEs:

$$\frac{dx}{dt} = \sigma(y - x),$$

$$\frac{dy}{dt} = x(\rho - z) - y,$$

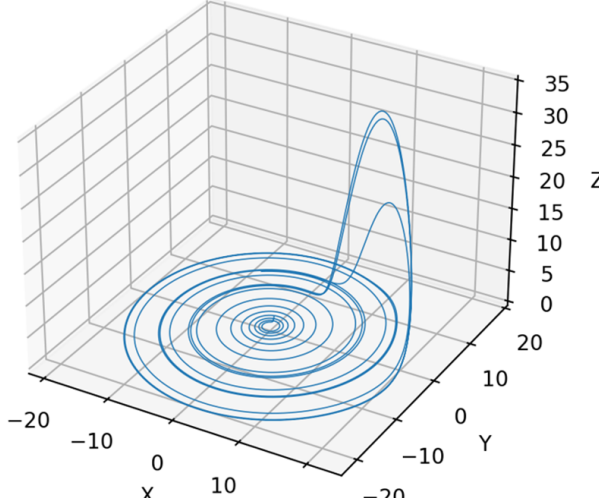
$$\frac{dz}{dt} = xy - \beta z,$$

The Rössler attractor similarly has three coupled ODEs:

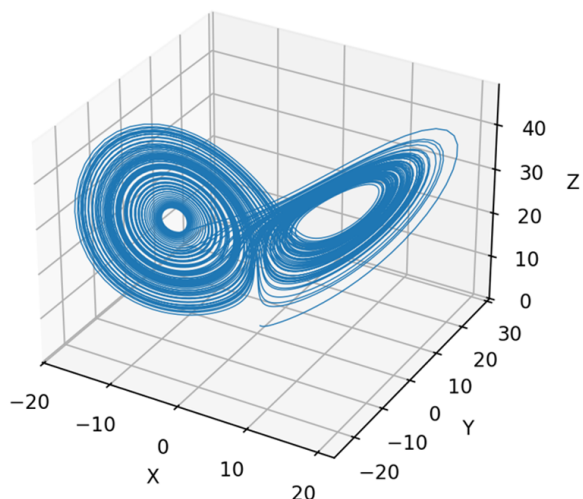
$$\frac{dx}{dt} = -y - z,$$

$$\frac{dy}{dt} = x + ay,$$

$$\frac{dz}{dt} = b + z(x - c),$$



(a)



(b)

FIG. 16. Two chaotic attractors that illustrate what chaos in the Bloch vector component might look like (a) Where  $\sigma = 10$ ,  $\beta = \frac{8}{3}$  and  $\rho = 28$ . (b) Where  $a = 0.1$ ,  $b = 0.1$  and  $c = 14$ .

- [1] F. Potter, A. Zagorskin, S. Savel'ev, and A. G. Balanov, Hysteresis and self-oscillations in an artificial memristive quantum neuron, *Physical review. A/Physical review, A* **110**, 10.1103/physreva.110.042604 (2024).
- [2] L. Chua, Memristor-the missing circuit element, *IEEE Transactions on Circuit Theory* **18**, 507 (1971).
- [3] R. Williams, How we found the missing memristor, *IEEE Spectrum* **45**, 28 (2008).
- [4] Y. Xiao, B. Jiang, X. Chen, S. Ke, Y. Jin, X. Wen, and C. Ye, A review of memristor: material and structure

design, device performance, applications and prospects, *Taylor Francis* **24**, 10.1080/14686996.2022.2162323 (2023).

- [5] G. Zhou, Z. Wang, B. Sun, F. Zhou, L. Sun, H. Zhao, X. Hu, X. Peng, J. Yan, H. Wang, W. Wang, J. Li, B. Yan, D. Kuang, Y. Wang, L. Wang, and S. Duan, Volatile and nonvolatile memristive devices for neuromorphic computing, *Advanced Electronic Materials* **8**, 2101127 (2022).
- [6] A. Akther, Y. Ushakov, A. G. Balanov, and S. E.

- Savel'ev, Deterministic modeling of the diffusive memristor, *Chaos: An Interdisciplinary Journal of Nonlinear Science* **31**, 10.1063/5.0056239 (2021).
- [7] H. Lv, X. Xu, P. Sun, H. Liu, Q. Luo, Q. Liu, W. Banerjee, H. Sun, S. Long, L. Li, and M. Liu, Atomic view of filament growth in electrochemical memristive elements, *Scientific Reports* **5**, 10.1038/srep13311 (2015).
- [8] M. Ismail, M. Rasheed, C. Mahata, M. Kang, and S. Kim, Mimicking biological synapses with a-hfsiox-based memristor: implications for artificial intelligence and memory applications, *Springer Nature* **10**, 10.1186/s40580-023-00380-8 (2023).
- [9] W. Chen, L. Song, S. Wang, Z. Zhang, G. Wang, G. Hu, and S. Gao, Essential characteristics of memristors for neuromorphic computing, *Advanced electronic materials* **9**, 10.1002/aelm.202200833 (2022).
- [10] K. Sun, J. Chen, and X. Yan, The future of memristors: Materials engineering and neural networks, *Advanced Functional Materials* **31**, 2006773 (2020).
- [11] K. Eshraghian, O. Kavehei, K.-R. Cho, J. M. Chappell, A. Iqbal, S. F. Al-Sarawi, and D. Abbott, Memristive device fundamentals and modeling: Applications to circuits and systems simulation, *Proceedings of the IEEE* **100**, 1991 (2012).
- [12] H. Lin, C. Wang, Q. Hong, and Y. Sun, A multi-stable memristor and its application in a neural network, *IEEE Transactions on Circuits and Systems II: Express Briefs* **67**, 3472 (2020).
- [13] X. Zou, S. Xu, X. Chen, L. Yan, and Y. Han, Breaking the von neumann bottleneck: architecture-level processing-in-memory technology, *Science China Information Sciences* **64**, 10.1007/s11432-020-3227-1 (2021).
- [14] N. Talati, R. Ben-Hur, N. Wald, A. Haj-Ali, J. Reuben, and S. Kvatinsky, mmpu—a real processing-in-memory architecture to combat the von neumann bottleneck, *Springer series in advanced microelectronics* **63**, 191 (2019).
- [15] C. D. Schuman, S. R. Kulkarni, M. Parsa, J. P. Mitchell, P. Date, and B. Kay, Opportunities for neuromorphic computing algorithms and applications, *Nature Computational Science* **2**, 10–19 (2022).
- [16] G. Indiveri, B. Linares-Barranco, R. Legenstein, G. Deligeorgis, and T. Prodromakis, Integration of nanoscale memristor synapses in neuromorphic computing architectures, *Nanotechnology* **24**, 384010 (2013).
- [17] Q. Lin, Y. Zhu, J. Sun, S. Peng, Z. Wang, K. You, X. Guo, Y. Wang, D. Li, L. Lin, Y. Zhao, Y. Liu, and F. Li, A full-quantum-dot optoelectronic memristor for in-sensor reservoir computing system with integrated functions, *Advanced Functional Materials* 10.1002/adfm.202423548 (2025).
- [18] M. Spagnolo, J. Morris, S. Piacentini, M. Antesberger, F. Massa, A. Crespi, F. Ceccarelli, R. Osellame, and P. Walther, Experimental photonic quantum memristor, *Nature Photonics* **16**, 318 (2022).
- [19] J. He, G. Zhou, B. Sun, L. Yan, X. Lang, Y. Yang, and H. Hao, Graphene quantum dots induced performance for intelligence memristors, *Nanoscale* **24**, 10.1039/d5nr00597c (2025).
- [20] D. Tian, C. Ke, B. Sun, H. Liang, Z. Qian, Q. Wen, X. Chen, C. Yang, M. Xu, and Y. Zhao, Quantum dot-based memristors for information processing and artificial intelligence applications, *Nanoscale* **17**, 10.1039/d5nr00136f (2025).
- [21] G. C. Adam, A. Khiat, and T. Prodromakis, Challenges hindering memristive neuromorphic hardware from going mainstream, *Nature Communications* **9**, 10.1038/s41467-018-07565-4 (2018).
- [22] K. C. Iarosz, E. C. Gabrick, J. Trobia, R. R. Borges, P. R. Protachevicz, R. C. Bonetti, Silvio, G. L. Batista, S. Jr., I. L. Caldas, and A. M. Batista, Chaotic dynamics in memristive circuits, *Revista Brasileira de Ensino de Física* **45**, 10.1590/1806-9126-rbef-2023-0116 (2023).
- [23] J.-M. Ginoux, B. Muthuswamy, R. Meucci, S. Euzzor, A. Di Garbo, and K. Ganeshan, A physical memristor based muthuswamy–chua–ginoux system, *Scientific Reports* **10**, 10.1038/s41598-020-76108-z (2020).
- [24] A. Ascoli, V. Lanza, F. Corinto, and R. Tetzlaff, Synchronization conditions in simple memristor neural networks, *Journal of the Franklin Institute* **352**, 3196 (2015).
- [25] Y. A. Kuznetsov, Andronov-hopf bifurcation, *Scholarpedia* **1**, 1858 (2006).
- [26] E. Marder and A. L. Taylor, Multiple models to capture the variability in biological neurons and networks, *Nature Neuroscience* **14**, 133 (2011).
- [27] H.-P. Breuer, The theory of open quantum systems (2025).
- [28] S. E. Savel'ev, F. Marchesoni, and A. M. Bratkovsky, Mesoscopic resistive switch: non-volatility, hysteresis and negative differential resistance, *The European Physical Journal B* **86**, 10.1140/epjb/e2013-40966-4 (2013).
- [29] D. Cohen and Y. Imry, Dephasing at low temperatures, *Physical Review B* **59**, 11143 (1999).
- [30] A. Balanov, *Synchronization* (Springer Berlin Heidelberg, 2009).
- [31] N. Inaba, Y. Nishio, and T. Endo, Chaos via torus breakdown from a four-dimensional autonomous oscillator with two diodes, *Physica D Nonlinear Phenomena* **240**, 903 (2011).
- [32] Y. Li, Z. Wang, R. Midya, Q. Xia, and J. J. Yang, Review of memristor devices in neuromorphic computing: materials sciences and device challenges, *Journal of Physics D: Applied Physics* **51**, 503002 (2018).